MEASUREMENT OF LOW-EMITTANCE BEAM WITH CODED APERTURE X RAY OPTICS AT CesrTA*

J.W. Flanagan†, H. Fukuma, H. Ikeda, T. Mitsuhashi, KEK, Tsukuba, Ibaraki 305-0801, Japan
G.S. Varner, U. Hawaii, Honolulu, HI 96822, USA
J.P. Alexander, N. Eggert, W.H. Hopkins, B. Kreis, M.A. Palmer, D.P. Peterson,
CLASSE, Cornell U., Ithaca, NY 14853, USA

Abstract

An x-ray beam size monitor based on coded aperture imaging [1] has been developed at CesrTA, for the purpose of making bunch-by-bunch, turn-by-turn measurements of low emittance beams. Using low-emittance beam we have been able to make detailed comparisons between the measured mask response and that predicted by theory, validating our simulations of the mask response. In turn, we demonstrate the ability to measure both integrated and single-bunch turn-by-turn beam sizes and positions for monitoring the progress of the low-emittance tuning of the machine, and for electron-cloud instability-related beam dynamics studies.

INTRODUCTION

Our goal is to develop an x-ray monitor for transverse bunch-by-bunch beam profile monitoring, with high resolution (a few μm), low beam-current dependence, and fast response, suitable for bunch-by-bunch diagnostics at present and future lepton accelerators, such as CesrTA, SuperKEKB, or the ILC damping ring. To meet these requirements, we are developing an x-ray imaging system based on coded aperture imaging [3], which consists of a pseudo-random array of pinholes that project a mosaic of pinhole camera images onto a detector. This image is then decoded using the known mask pattern to reconstruct the original image. One example of such a pattern is the coded aperture pattern used at CesrTA, a Uniformly Redundant Array (URA) [4], which features an open aperture of 50% with an even sampling of spatial frequencies in the non-diffractive limit. The mask, shown in Fig. 1, is composed of $0.55\,\mu$m Au in the mask regions, on a $2.5\,\mu$m Si substrate. It was made by Applied Nanotools, Inc. The minimum vertical feature size is $10\,\mu$m, with a horizontal width of $1200\,\mu$m.

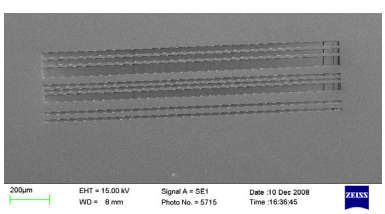

Figure 1: Coded aperture test mask used for beam test at CesrTA. (SEM courtesy of Applied Nanotools, Inc.)

* Work supported in part by the Japan/US Cooperation Program
† john.flanagan@kek.jp

BEAM LINE, DETECTOR

The beam line used for these tests was the CHESS D Line, viewing a 2.085 GeV positron beam. The x-ray optics (coded aperture mask, Fresnel zone plate, movable slits) are mounted in a holder 4.29 m downstream of the beam, with the detector a further 10.25 m downstram from the optics holder. The beam line is evacuated from beam source point to detector, with a 4.15μm diamond window located just upstream of the detector, to separate the vacuum on the detector side from the clean vacuum on the beam side. The detector is an InGaAs array produced by Fermionics, Inc., which features $25\,\mu$m $\times 500\,\mu$m pixels on a $50\,\mu$m pitch. Pinhole scans across the surface indicate that the pixels effectively behaves as though they are $50\,\mu$m wide. The thickness of the InGaAs layer is $3.5\,\mu$m, which captures about 90% of the flux that reaches it after passing through the diamond window, and other layers on the chip above the InGaAs layer. The detectable spectrum lies largely between 1 and 5 keV.

A high-speed readout has been developed capable of bunch-by-bunch, turn-by-turn digitization at CesrTA [5]. These data are called "snapshots." One issue with the snapshot data is that the inter-pixel calibration is not yet fully satisfactory; for this reason, raw, uncalibrated snapshot data data are used in this paper. For preliminary checking of the x-ray system [6] and beam sizes, a single Fermionics pixel is mechanically scanned across the imaging plane while being read out in DC mode with a picoammeter. These data are called "slow scans."

The data were taken the week of May 10, 2010, and should be considered still somewhat preliminary.

LOW-EMITTANCE BEAM MEASUREMENTS

Simulation Validation with Slow Scans

As has been described in detail previously [2], the expected image at the detector plane is calculated starting from the σ and π components of the complex wavefront amplitude of the component of synchrotron radiation (SR) with angular frequency ω [7],

$$\begin{bmatrix} A_\sigma \\ A_\pi \end{bmatrix} = \frac{\sqrt{3}}{2\pi}\gamma\frac{\omega}{\omega_c}\left(1+X^2\right)(-i)\begin{bmatrix} K_{2/3}(\eta) \\ \frac{iX}{\sqrt{1+X^2}}K_{1/3}(\eta) \end{bmatrix}.$$

We propagate the wavefronts $A_{\sigma,\pi}$ through a model of the beamline, taking account of the attenuation and phase shifts

due to the various materials and pathlengths along the way, with a Kirchhoff integral over the surface of the mask [8]:

$$A_{\sigma,\pi}(y_d) = \frac{iA_{\sigma,\pi}(\text{source})}{\lambda} \int_{\text{mask}} \frac{t(y_m)}{r_1 r_2} e^{i\frac{2\pi}{\lambda}(r_1+r_2)} \times \left(\frac{\cos\theta_1 + \cos\theta_2}{2}\right) \mathrm{d}y_m.$$

For each pixel in the detector, the wavefront amplitude from each source point is calculated by the above integral, and converted to detected flux. The weighted flux contributions from source points are then summed over the source distribution. This process is repeated over the detectable spectral range, taking into account the material properties of the detector. By varying the weighting of source points and comparing the resulting image against data, the source profile can be reconstructed. For fast fitting (as shown in this paper), a series of templates are generated for a range of beam sizes and position offsets, which are then compared against the data to find the closest match.

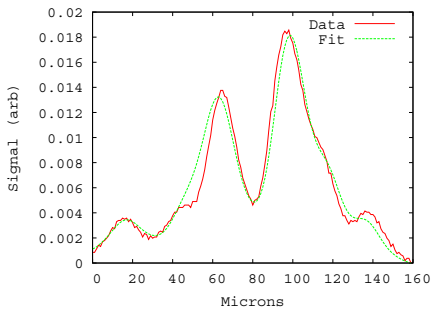

Figure 2: Slow scan: Detector image data, and best fit simulated image of 25 μm beam.

In previous measurements [2], a discrepancy in the number of features had been reported between data and simulation for a 1-dimensional simulation. Since that time, it was found that widening the integration limits over the mask surface in the mask integral gave very good agreement between data and simulated image features for the one-dimensional source simulation.

Bunch-by-bunch, Turn-by-turn Measurements

The best fit to the slow scan data is 25 μm, while that of the fast snapshot data is 18.8 ± 0.1 μm. The fast snapshot data also show a beam centroid motion of 7.8 ± 0.1 μm in RMS, which taken in quadrature with the beam size implies a smeared beam size of 20.4 μm. These data were taken over ∼200 turns. However, in addition, there was also a ~ 10 μm slow orbit "wobble," which would give a smeared beam size of $\sim$ 23 μm, close to that found by the slow scan. Further calibration cross-checks are planned. Figure 3 shows the turn-by-turn size and position of the first bunch in the train; betatron motion can be observed in the position data. Figure 4 shows the bunch-by-bunch sizes and RMS position amplitudes, measured turn-by-turn and averaged

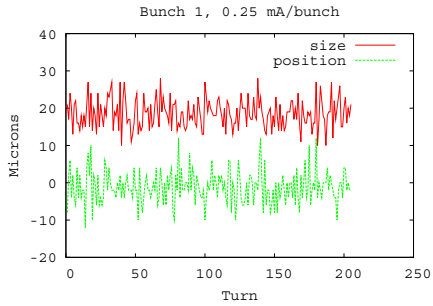

Figure 3: Bunch 1, turn-by-turn sizes and position measurements on 2.085 GeV beam with coded aperture.

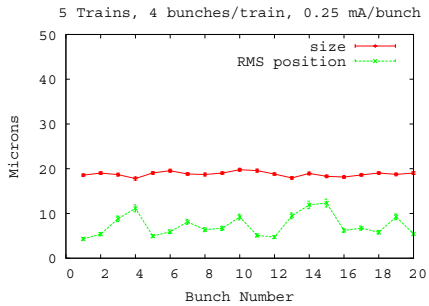

Figure 4: Turn-averaged sizes and RMS position spreads for 20 bunches, with statistical error bars shown.

over ∼200 turns. The error bars shown are the statistical uncertainties in the means.

To test the ability to distinguish different beam sizes, a coupling knob ("betasing1") was used to blow up the beam in steps. The results are shown in Figure 5. At each knob setting, the single-bunch beam sizes are measured turn-by-turn, then the measurements are averaged together. The minimum beam size was expected to be at a knob setting of zero units; the actual minimum appears to be a bit to the right of there.

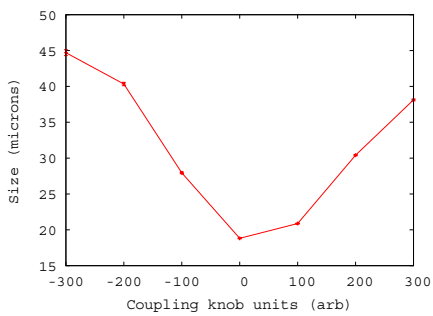

Figure 5: Bunch sizes measured for different values of coupling knob ("betasing1"). Single-turn, single-bunch sizes are averaged over ∼200 turns. Statistical error bars shown.

Instability Study Measurements

An attempt was made to measure the effect of electron-clouds on the bunch-by-bunch beam size. For this purpose, a train of 45 bunches was stored in the ring, at 14 ns spacing, and the currents gradually raised. Shown in Figures 6 and 7 are the turn-averaged bunch sizes and RMS position amplitudes along the train for the cases of 0.5 mA/bunch and 1.0 mA/bunch. As can be seen, at the higher bunch current a pronounced bunch blow-up occurs, which may be due to electron clouds, and a size increase is also seen at the head of the train, the cause of which is not yet understood [9]. Bunch-by-bunch lifetimes showed a similar pattern along the train to the beam sizes measured here, with smaller bunches having shorter lifetimes. Analysis of the data are still ongoing, but these plots demonstrate the ability of the coded aperture to measure a range of bunch-by-bunch beam sizes. Figure 8 shows the fit to a single turn of

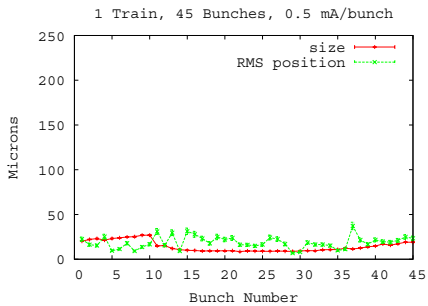

Figure 6: Sizes and positions along train of 45 bunches at 0.5 mA/bunch.

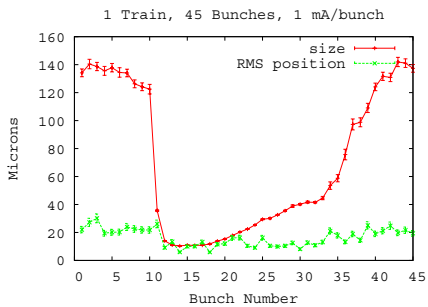

Figure 7: Sizes and positions along train of 45 bunches at 1.0 mA/bunch.

Bunch 15 at 1.0 mA/bunch. The turn-averaged beam size (over 100 turns) for this bunch is $11.0\ \mu\text{m} \pm 0.2\ \mu\text{m}$, which is consistent with a vertical emittance of 20 pm, the target emittance of CesrTA. However, this should be considered still a preliminary result.

SUMMARY AND REMAINING ISSUES

Measurements have been taken with a coded aperture mask at CesrTA in both slow scan and single-shot (bunch-by-bunch, turn-by-turn) modes. The slow scans validate

Figure 8: Single-shot data and fit for Bunch 15 at 1.0 mA/bunch. Best fit size: 11 μm.

the beam simulations, and the fast snapshots demonstrate the ability to measure size and position of bunch trains on a bunch-by-bunch and turn-by-turn basis. The slow scans and fast snapshots generally agree on relative sizes, with some uncertainty in the absolute measurements due to possible the presence of a slow orbit wobble. Quantitative work on analysis of the data is still underway. Further detector inter-pixel calibration work is needed, and the testing of new mask designs capable of measuring higher energy beams, and also designs with potentially smaller resolution, is planned. Development is also underway on detectors with finer spatial and timing resolution.

ACKNOWLEDGMENTS

We would like to thank Aaron Lyndaker, Ernie Fontes, Mike Billing, Jim Shanks, Michael Forster and others at the CesrTA/CHESS facility for their assistance in carrying out these measurements. Parts of this research are supported by the Japan Ministry of Education, Culture, Sports, Science and Technology (Monbukagakusho), and by the Japan/US Cooperation Program, and CesrTA is supported by the US DOE (DE-FC02-08ER41538) and NSF (PHY-0734867).

REFERENCES

[1] J.W. Flanagan *et al.*, Proc. EPAC08, Genoa, 1029 (2008).

[2] J.W. Flanagan *et al.*, Proc. PAC09, Vancouver, (2009).

[3] R.H. Dicke, Astrophys. Journ., **153**, L101, (1968).

[4] E.E. Fenimore and T.M. Cannon, Appl. Optics, V17, No. 3, p. 337 (1978).

[5] J.P. Alexander *et al.*, Proc. PAC09, Vancouver, (2009).

[6] W. Hopkins *et al.*, Proc. PAC09, Vancouver, (2009).

[7] K.J. Kim, AIP Conf. Proc 184 (1989).

[8] J.D. Jackson, "Classical Electrodynamics," (Second Edition), John Wiley & Sons, New York (1975).

[9] M. Billing, private communication.